INTERNATIONAL JOURNAL OF
ENERGY RESEARCH

A Short Chemical-Kinetic Nitrogen Mechanism for Carbon-Free Combustion, Including Ammonia Autoignition and Deflagration, with Application to Gas-Turbine-Relevant Flame Characteristics

Journal:	*International Journal of Energy Research*
Manuscript ID	ER-19-12511.R1
Wiley - Manuscript type:	Research Article
Date Submitted by the Author:	n/a
Complete List of Authors:	Jiang, Yuanjie; University of California San Diego, Mechanical and Aerospace Engineering Gruber, Andrea; SINTEF Energy Research Seshadri, Kalyanasundaram; University of California San Diego, Mechanical and Aerospace Engineering Williams, Forman; University of California San Diego, Mechanical and Aerospace Engineering
Keywords:	NH3-H2, Nitrogen, Chemical-kinetic mechanism, Ammonia combustion, NOx formation

Received: Added at production | Revised: Added at production | Accepted: Added at production

DOI: xxx/xxxx

RESEARCH ARTICLE

A Short Chemical-Kinetic Nitrogen Mechanism for Carbon-Free Combustion, Including Ammonia Autoignition and Deflagration, with Application to Gas-Turbine-Relevant Flame Characteristics

Yuanjie Jiang*[1] | Andrea Gruber[2] | Kalyanasundaram Seshadri[1] | Forman A. Williams[1]

[1]Department of Mechanical and Aerospace Engineering, University of California San Diego, CA, USA
[2]SINTEF Energy Research, Trondheim, Norway

Correspondence
*Yuanjie Jiang
Email: yuj056@ucsd.edu

Present Address
Engineering Building II (EBU II) Room 564
9500 Gilman Drive

Summary

Chemical-kinetic combustion mechanisms for hydrogen-oxygen-nitrogen systems, motivated originally by concerns about NOx emissions during hydrogen burning, have recently acquired renewed interest as a result of the possibility of employing ammonia-hydrogen mixtures in gas turbines as drop-in fuel to replace the use of natural gas. Specifically, this is of relevance to the implementation of engineering approaches for economical power generation with carbon sequestration or to large-scale energy-storage schemes, based on hydrogen or efficient hydrogen carriers such as ammonia. Because computational investigations are facilitated by short mechanisms (since the use of large mechanisms often is prohibitively expensive), in response to the original concerns a short nitrogen mechanism was developed in San Diego in the 1990's (not up-dated since 2004), without consideration of ammonia combustion. In view of the renewed interest, that mechanism has now been expanded to encompass 60 elementary steps among 19 reactive chemical species, including ammonia burning (along with NOx production), as reported herein, providing predictions sufficiently accurate for many purposes. Although less accurate in certain respects than predictions of much larger mechanisms, the present short mechanism retains satisfactory accuracy at gas-turbine conditions, and it can be efficiently utilized in large-scale CFD calculations that cannot practically employ larger mechanisms. The revisions maintain the shortness of the original mechanism, adding only one more reactive species and six more elementary steps (while updating values of rate parameters of nine other steps, on the basis of newly available information). The performance of the new mechanism is documented here through comparisons of its predictions with experimental data. Furthermore, the short mechanism is applied herein to the analysis of fundamental combustion properties of ammonia/hydrogen/nitrogen-air laminar premixed flames, at unstrained and strained conditions, for comparison with methane-air flames as a reference gas-turbine fuel.

KEYWORDS:
NH_3-H_2, Nitrogen, Chemical-kinetic mechanism, Ammonia combustion, NOx formation

1 | INTRODUCTION

Among the many strategies currently being pursued to reduce the dependence on fossil fuels in fulfilling energy needs is the use of hydrogen as an energy carrier. This approach is relevant both to power generation with pre-combustion carbon sequestration, where hydrogen is produced at large scale from natural gas in conjunction with CO_2 capture and storage[1], and to large-scale energy-storage schemes, where hydrogen is produced from water electrolysis using intermittent excess power from non-dispatchable renewable energy sources (wind, sun)[2]. Because of its much higher boiling point than that of hydrogen and the well-developed technology for its production, transportation, and storage (a result of the long history of its widespread utilization in agriculture), ammonia is being considered as a viable and economic alternative to liquefied or highly compressed hydrogen as a carbon-free energy carrier. In connection with this and other applications, combustion of fuels consisting of mixtures of ammonia and hydrogen are under investigation within industrial demonstration efforts[†]. While a number of early studies have indicated an obvious inadequacy of neat ammonia as a gas-turbine fuel[3], mostly due to its poor reactivity compared to more conventional hydrocarbons, partial cracking of ammonia to form opportunely selected mixtures of ammonia, hydrogen and nitrogen has a good potential to improve the overall fuel reactivity and its combustion performance in gas turbines designed for use with natural gas. Ammonia, which also is essential to catalytic de-NOx chemistry for exhaust cleaning, has, in addition, been considered for direct use in reciprocating engines[4]. Production of oxides of nitrogen through fuel chemistry in the combustion of ammonia often is, however, a detriment requiring study of its mitigation.

These considerations have focused attention on current uncertainties in the combustion chemistry of ammonia, resulting in recent evaluations of that chemistry[5,6,7]. The chemical-kinetic mechanisms studied in this recent work generally involve hundreds of elementary steps, typically preventing their direct use in computational fluid dynamics, as is required in the design and evaluation fluid-flow and power-production equipment and processes. Not all of the elementary steps and chemical species in those mechanisms, however, influence predicted combustion characteristics appreciably. It therefore is possible to extract subsets of the elementary reactions that are short enough to be readily employed computationally yet accurate enough to produce reasonable predictions. The objective of the present work is to derive a short mechanism for the combustion of ammonia and hydrogen that is suitable for large-scale computational investigations.

Accomplishment of this objective was facilitated by the existence, in the short San Diego mechanism[8], of a nitrogen-chemistry component that included 54 carbon-free elementary steps among 18 reactive chemical species, as part of a sub-mechanism for predicting NOx emissions in hydrocarbon flames. That mechanism had been shown to perform reasonably well for hydrogen and some hydrocarbon flames (as well as methanol, dimethyl ether, and hydrogen mixed with nitrogen dioxide or methane)[9,10,11,12,13,14,15], but it had not addressed the combustion of ammonia. In the present work, through rate-constant comparisons, sensitivity analysis, and comparisons with more recently available experiments, it was found that, after up-dating rate parameters on the basis of more recent reaction-rate investigations, augmentation of the mechanism through addition of only one more reactive species and six more reaction steps was sufficient to derive an up-dated San Diego mechanism that extends its capabilities to cover ammonia combustion as well.

To evaluate the performance of this new mechanism, its predictions are compared here with results of experiments on the combustion of ammonia and of its mixtures with hydrogen. All of the relevant available combustion experiments are studied. These include shock-tube and rapid-compression-machine measurements of ignition delay times, burning velocities of stabilized and spherically expanding laminar premixed flames, strain rates at extinction of counterflow premixed and diffusion flames, laminar premixed flame structures with emphasis on NO concentration profiles, and NOx emissions in experiments employing laminar premixed flame. The comparisons show that, in many respects, the updated mechanism performs much better than the original short mechanism on which it was based.

Finally, deploying the newly updated mechanism in a first application, we investigate the fundamental combustion properties of ammonia/hydrogen/nitrogen gaseous fuel mixtures resulting from partial ammonia dissociation and perform numerical simulations of unstrained and strained laminar premixed flames, for comparison with methane, a well-established gas-turbine reference gaseous fuel. This investigation reveals previously unanticipated blow-out characteristics of the carbon-free blend that require consideration in practical applications.

[†]BIGH2/Phase III - "Enabling safe, clean and efficient utilization of hydrogen and ammonia as the carbon-free fuels of the future" - CLIMIT-Demo Project Number 617137 performed by SINTEF, NTNU, Siemens Industrial Turbomachinery and Equinor.

TABLE 1 Proposed New San Diego Nitrogen Chemistry.

Reaction		A	n	E	Reference	Note
1. $O+N_2=NO+N$		1.47×10^{13}	0.3	75286.81		
2. $N+O_2=NO+O$		6.40×10^{9}	1	6285.85		
3. $N+OH=NO+H$		3.80×10^{13}	0	0		
4. $NH+H=N+H_2$		1.00×10^{14}	0	0	16	Changed
5. $NH+O=NO+H$		9.20×10^{13}	0	0		
6. $NH+OH=HNO+H$		4.00×10^{13}	0	0		
7. $NH+OH=N+H_2O$		5.00×10^{11}	0.5	2000.48		
8. $NH+O_2=HNO+O$		4.60×10^{5}	2	6500.96		
9. $NH+NO=N_2O+H$		1.80×10^{14}	-0.351	-244	17	Changed
10. $NH+NO=N_2+OH$		2.20×10^{13}	-0.23	0		
11. $NH_2+H=NH+H_2$		4.00×10^{13}	0	3652.01		
12. $NH_2+O=HNO+H$		6.60×10^{14}	-0.5	0	18	Changed
13. $NH_2+O_2=H_2NO+O$		2.60×10^{11}	0.4872	29050	17	Added
14. $NH_2+OH=NH+H_2O$		4.00×10^{6}	2	1001.43		
15. $NH_2+N=N_2+H+H$		7.00×10^{13}	0	0	18	Added
16. $NH_2+NO=N_2+H_2O$		2.80×10^{20}	-2.654	1258	17	Changed
17. $NH_2+NO=N_2H+OH$		3.10×10^{13}	-0.48	1180		
18. $NH_3+M=NH_2+H+M^{\ddagger}$		2.20×10^{16}	0	93451.24		
19. $NH_3+H=NH_2+H_2$		6.40×10^{5}	2.39	10181.64		
20. $NH_3+O=NH_2+OH$		9.40×10^{6}	1.94	6465.11		
21. $NH_3+OH=NH_2+H_2O$		2.04×10^{6}	2.04	566.44		
22. $N_2H+O_2=N_2+HO_2$		2.00×10^{14}	0	0	18	Added
23. $N_2H(+M)=N_2+H(+M)^{\S}$	k_∞	6.50×10^{7}	0	0	19	Changed
	k_0	5.00×10^{13}	0	0		
24. $N_2H+H=N_2+H_2$		1.00×10^{14}	0	0		
25. $N_2H+O=N_2O+H$		1.00×10^{14}	0	0		
26. $N_2H+OH=N_2+H_2O$		5.00×10^{13}	0	0		
27. $H+NO+M=HNO+M^{\P}$	k_∞	1.50×10^{15}	-0.4	0	20	Changed
	k_0	4.30×10^{14}	0.206	-1554.97		
28. $HNO+H=NO+H_2$		4.40×10^{11}	0.72	650.1		
29. $HNO+OH=NO+H_2O$		3.60×10^{13}	0	0		
30. $N_2O(+M)=N_2+O(+M)^{\#}$	k_∞	8.00×10^{11}	0	62619.5		
	k_0	2×10^{14}	0	56644.36		
31. $N_2O+H=N_2+OH$		3.31×10^{10}	0	5090	21	Changed
Bi-Arrhenius		7.83×10^{14}	0	19390		
32. $N_2O+O=2\ NO$		9.15×10^{13}	0	27693	22	Changed
33. $N_2O+OH=N_2+HO_2$		2.00×10^{13}	0	40000	23	Changed
34. $NO_2+M=NO+O+M^{\|\|}$		1.10×10^{16}	0	65965.58		
35. $NO+HO_2=NO_2+OH$		2.10×10^{12}	0	-480.4		
36. $NO_2+H=NO+OH$		3.50×10^{14}	0	1500.96		
37. $NO_2+O=NO+O_2$		1.00×10^{13}	0	599.9		
38. $H_2NO+O=HNO+OH$		3.00×10^{7}	2	2000	18	Added
39. $H_2NO+O_2=HNO+HO_2$		3.00×10^{12}	0	25000	19	Added
40. $H_2NO+HO_2=HNO+H_2O_2$		2.90×10^{4}	2.69	-1600	24	Added

Units are cm^3, mol, s, cal, K; reaction-rate constants are $k_f = AT^n \exp(-E/RT)$.

[1,2,4] Chaperon efficiencies are unity.

[3] The efficiency factors are $\epsilon_{AR} = 0.50$, $\epsilon_{H_2O} = 5.00$, with others unity.

[5] The only efficiency factor different from unity is $\epsilon_{H_2O} = 16.25$.

[2,3,4] Rates are in the Lindemann Falloff form.

2 | UP-DATED NITROGEN CHEMISTRY

Table 1 lists the 40 nitrogen-containing steps of the new mechanism, along with their associated forward rate parameters; the reverse rate constants are to be calculated from the forward rate constants and the equilibrium constants. The rate parameters for entries without notation in the table are the same as those of the original mechanism. The revisions that have been made now will be discussed sequentially.

The change in entry 4 significantly improves agreement with shock-tube measurements[25], as pointed out in recent autoignition work[26]. The new value of this rate, an upper limit for the collision rate, is taken from an earlier reference than that selected previously for the mechanism, and it exceeds a recent recommendation[27] by a factor of three and the previous value appearing in the mechanism by an order of magnitude. The change in entry 9, on the other hand, is small, reflecting a small increase based on newer results that are justified in a recent evaluation[26]. In entry 12, similarly[26], newer results indicate a small decrease.

Entry 13 produces a radical that was not present in the previous mechanism but that is very important in the autoignition of ammonia[26]. The introduction of this radical requires the addition of the last three steps in the table, reflecting its role in the production of HNO. In the absence of this path, the production rate of HNO is too small, especially at lower temperatures, leading to predicted ignition delay times that are much too long.

The addition of entry 15 is important for improving predictions of burning velocities of mixtures of ammonia and hydrogen, especially for stoichiometric and fuel-rich conditions, where the previous predicted velocities were much too low. This step affords significant additional chain branching under those conditions.

For entry 16, the updated rate parameters shown have produced excellent agreement with experimental measurements[28,29]; the new rate constant is slightly higher than that of the previous mechanism. Entry 22, of importance because of its competition with the dissociation reaction in entry 23, was not previously present and therefore now is added. Also previously, only the high-pressure limit was present for entry 23, but its falloff is important and therefore is now included, so the revisions in entries 22 and 23 now contribute to a better description of the fate of NNH. Falloff also can be important in entry 27, where previously only the low-pressure limit was employed.

Entry 31 is now known to be bi-Arrhenius, with different low-temperature and high-temperature pathways, a possibility that had been excluded in the previous mechanism, where only a high-temperature path had been included. Finally, the activation energies for entries 32 and 33 previously were a little too low, a deficiency now corrected on the basis on newer information.

3 | COMPARISONS WITH EXPERIMENT

The comparisons discussed here extend over a wide range of experimental data, including shock-tube ignition delay times (τ_{ign}), laminar burning velocities (S_L), premixed counterflow extinction strain rates (a_{ext}), and NO_x formation (mole fraction X_{NO_x}). The Cantera software[30] with Python interface was used in the computations. Data from shock tubes and rapid-compression machines, from freely propagating and burner-stabilized flames, from counterflow flames with plug-flow and potential-flow boundary conditions, and from stabilized burner flames were applied to investigate τ_{ign}, S_L, a_{ext}, and X_{NO_x} respectively. Premixed systems are characterized by the equivalence ratio, ϕ, defined on the basis of complete combustion of the reactants to carbon dioxide (CO_2), water (H_2O), and nitrogen(N_2).

3.1 | Ignition Delay Time

Fig.1 shows a comparison of the experimental data obtained by Pochet et al.[31] with computational results for ignition delay times in air (with some of the nitrogen replaced by argon to improve compression) of fuel-lean NH_3 with different amounts of H_2 addition. The ignition delay time is defined experimentally as the time between attainment of the maximum compression pressure and the maximum rate of pressure rise in the rapid-compression machine. As shown in the figure, the updated San Diego mechanism agrees much better with the experimental data than the previous mechanism, especially for pure NH_3, where the previous San Diego mechanism over-estimates τ_{ign} by four orders of magnitude! Computations employing other mechanisms in the literature revealed less discrepancy between the new predictions and experiments than had been found for the mechanisms in[32,33,34,35], which were over-reactive by amounts up to a factor of five under these conditions. These results provide strong support for the present revisions.

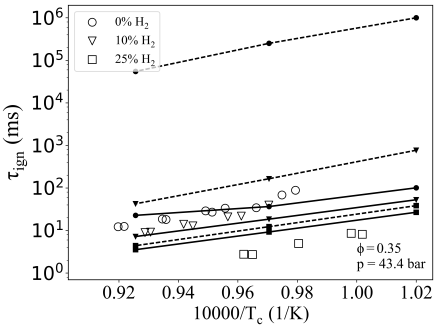

FIGURE 1 Ignition delay time of NH_3/H_2 mixtures in a rapid-compression machine for an equivalence ratio of 0.35 and a compression pressure of 43.4 bar[31]. Open symbols represent the experimental data, solid lines stand for the updated mechanism, and dashed lines are for the previous San Diego mechanism, conventions to be retained in all figures. Solid symbols along each line identify the corresponding H_2 content.

While the rapid-compression machine approximates well conditions of practical interest, shock-tube experiments often employ large excesses of argon or helium to improve the fidelity of fundamental data. In Fig.2, results are shown for experiments testing ignition delay times of premixed NH_3/O_2/Ar mixture, highly diluted (98% - 99% Ar dilution), in a shock tube, as reported by Mathieu et al.[26]. The ignition delay time was defined experimentally as the time at which a straight line tangent to the steepest rate-of-change of OH* chemiluminescent emission intensity reaches zero. Since the updated San Diego mechanism does not track OH*, computationally the ignition time was defined as the time at which the concentration of NH_2 reaches maximum, following a previous suggestion[35], which produces slightly better agreement with experiment than the maximum OH concentration. It may be seen in Fig.2a and in Fig.2b that the modified San Diego mechanism reproduces the trend of the experimental data much better than the previous mechanism. Although still somewhat under-reactive, not agreeing as well as the predictions of the much larger mechanism developed in[26] (not shown here), the differences remain within a factor of 2.

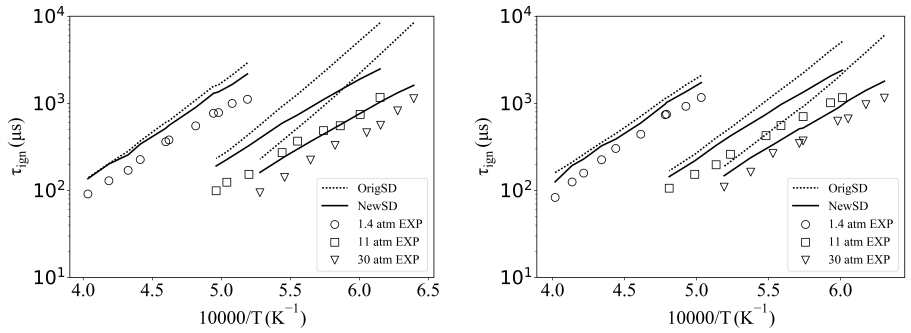

FIGURE 2 Ignition delay time of (a) 0.4% NH_3/0.6% H_2/99% Ar and (b) 0.5715% NH_3/0.4285% H_2/99% Ar mixtures in shock tube for an equivalence ratio of 0.5 and pressures of 1.4 atm, 11 atm, and 30 atm[26].

3.2 | Laminar Burning Velocity

In Fig.3, comparisons are shown for the laminar burning velocity. In the experiment[5], premixed NH_3/H_2/Air flames were stabilized in a tube-type burner with different NH_3/H_2 ratios and different equivalence ratios, at normal atmospheric pressure. The fresh mixtures were fed in at room temperature. The computations were performed for freely propagating laminar premixed flat flames of NH_3/H_2/Air. An adaptive grid was imposed to guarantee convergence of the flame-speed values. At the highest

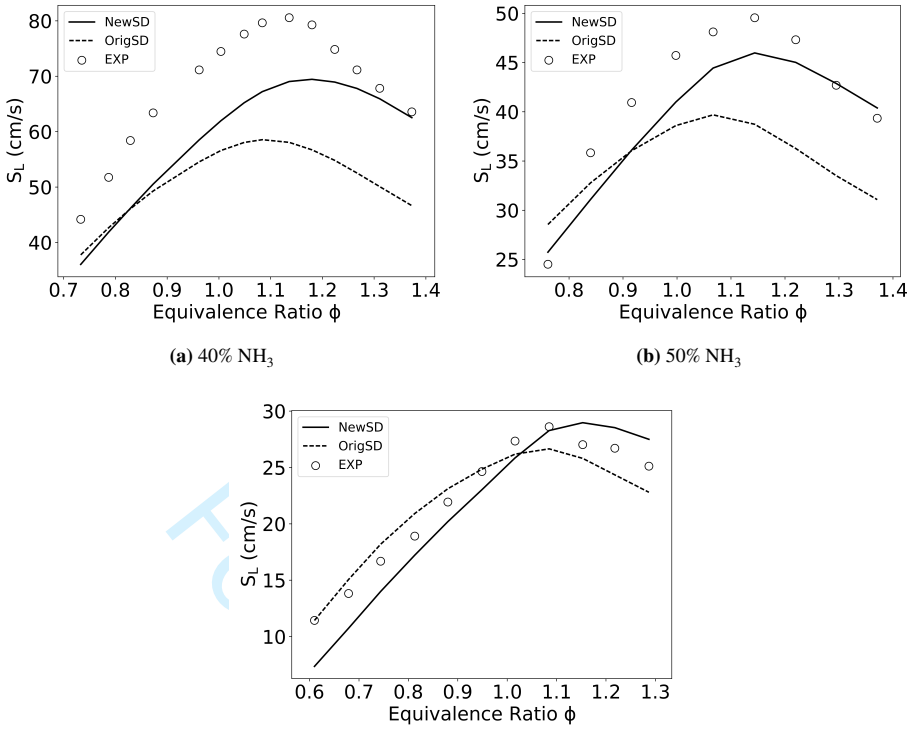

(a) 40% NH_3 **(b)** 50% NH_3

(c) 61.5% NH_3

FIGURE 3 Equivalence-ratio dependence of laminar burning velocities of (a) 40% NH_3/60% H_2, (b) 50% NH_3/50% H_2, and (c) 61.5% NH_3/38.5% H_2 in air at a pressure of 1 atm, for mixtures initially at room temperature[5].

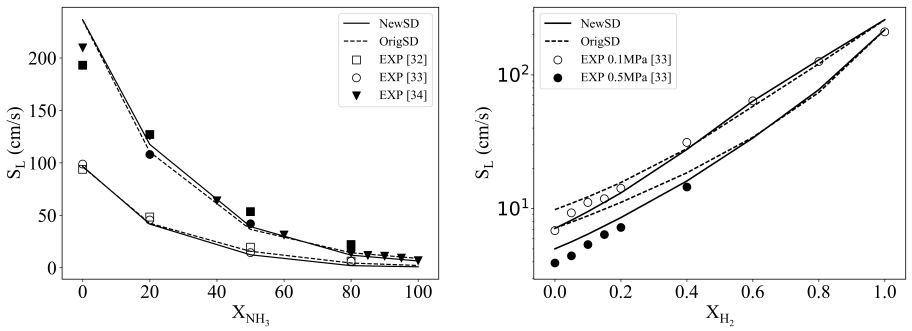

(a) p = 1 atm, $T = 298K$ **(b)** $\phi = 1$, $T = 298K$

FIGURE 4 Laminar burning velocities of NH_3/H_2/Air mixtures in closed chambers initially at room temperature (298 K)[36,37]. (a) Initial pressure is 0.1 MPa. Open symbols are for an equivalence ratio ϕ of 0.6, and black symbols are for ϕ=1 (stoichiometric conditions); burner-stabilized measurements[38] are seen to agree. (b) For stiochiometric mixtures[37], open symbols are for 0.1 MPa and black symbols are for 0.5 MPa.

equivalence ratios, where the effect of the fuel should be greatest, the figure shows increasing agreement between predictions and measurements with increasing hydrogen content, suggesting that the observed disagreements may be associated with the ammonia chemistry. The new mechanism is seen to afford noticeably improved agreement with experiment for stiochiometric and fuel-rich conditions. The consistent under-prediction of measured burning velocities at fuel-lean conditions may be related to the fact that, in the experiment, to be sure to avoid condensation of ammonia, the burner tube was heated to 423 K, and the

walls of the chamber enclosing the experiment were heated to 532 K, the higher temperatures possibly leading to higher burning velocities.

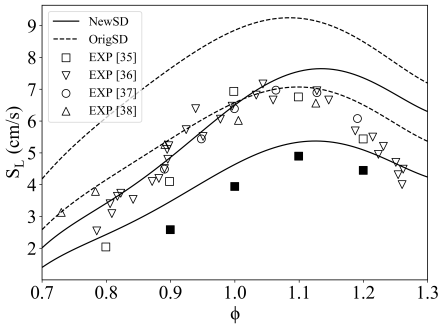

FIGURE 5 Laminar burning velocities of pure NH_3 in air measured in a constant-volume chamber at normal and elevated pressure (0.1 MPa and 0.5 MPa) with varying equivalence ratios ϕ[39,40,41,42]. Symbols represent the experimental measurements, open for 0.1 MPa and black for 0.5 MPa; solid curves stand for the updated mechanism and dashed for the original.

Measurements of spherically expanding laminar flames in closed chambers also provided burning-velocity data[36,37]. The results for normal atmospheric pressure, shown in Fig.4a, are seen to agree well with predictions of both the original mechanism (dashed curves) and the new mechanism (solid curves), practically all the way from pure ammonia fuel to pure hydrogen fuel under these conditions, although over-predictions for stoichiometric conditions may be seen for pure hydrogen. Although the adiabatic flame temperature decreases somewhat with increasing ammonia mole fractions, the decreasing burning velocity with increasing ammonia mole fraction, seen in this figure, results mainly from the decreasing reactivity associated with the reduced hydrogen content. Similar agreements were found at elevated pressures, as shown in Fig.4b, where the agreement begins to deteriorate as the ammonia content is increased beyond fifty percent, with over-predictions approaching a factor of two for pure ammonia. The new mechanism is seen here to improve the predictions appreciably for pure ammonia. This behavior for pure ammonia is seen in Fig.5 to extend to other equivalence ratios, where the improvement provided by the new mechanism is evident, although the predicted dependence on the equivalence ratio in fuel-rich mixtures seems to be appreciably weaker than was observed experimentally, despite some differences between different measurements.

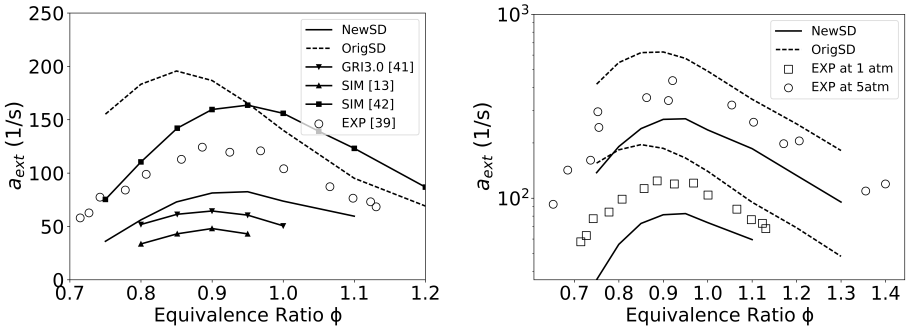

(a) T = 300 K, p = 1 atm **(b)** T = 300 K, p = 1, 5 atm

FIGURE 6 The variation with equivalence ratio of the extinction strain rate of NH_3/Air twin flames at (a) 1 atm and (b) 1 atm and 5 atm. Symbols represents the experiments[43], the solid curves provide the numerical predictions for the up-dated San Diego mechanism and the dashed curves for the previous mechanism, with curves also shown in (a) for three other mechanisms in the literature.

3.3 | Extinction Strain Rate

Experimental results are available for extinction strain rates of counterflow non-premixed NH_3/H_2 flames against air at normal atmospheric pressure and elevated temperatures[44] and of ammonia-air counterflow back-to-back premixed flames over a wide range of pressures and equivalence ratios[43]. In the first set of experiments[44], the mole fraction of NH_3 in the fuel mixture ranged from 0.88 to 0.99, and measurements were made at inlet temperatures from 348 K to 495 K. To stabilize the flames, honeycombs and beads were employed at the nozzle exits, providing approximately uniform exit velocities, but the separation distance of the nozzles exceeded the nozzle diameters, necessarily complicating the flow field on the oxidizer side of the stagnation plane where the flames were stabilized. As a result, plug-flow (uniform-exit-velocity) computations with one-dimensional temperature and composition fields and flow fields applicable at small ratios of separation distances to exit diameters failed to agree with the data, producing lower extinction strain rates and a much milder increase of the extinction strain rate with decreasing ammonia-to-hydrogen ratios than observed experimentally. For example, at 348 K and NH_3 mole fractions of 0.97 to 0.99, where the extinction strain rates are the lowest, so that the spatial strain-rate variations are minimized, the original mechanism agreed with the data, but the new mechanism gave extinction strain rates about half as large as observed. These differences may be attributed to the computations providing much larger strain rates at the flame than were present in the experiments, where strain rates near the plug-flow oxidizer exit would be expected to be small; fully two-dimensional computations of these specific experimental configurations (not available to us) would be required to test predictions for these experiments properly, whence comparisons are not shown here.

The pure-ammonia premixed twin-flame experiments[43] employed contoured nozzles without inserts, with reported strain rates appropriate for application of potential-flow boundary conditions, which were used in the computations. Largely because of the low strain rates in the experiments (barely high enough to avoid the necessity of introducing buoyancy corrections), fully two-dimensional computations are not needed for making proper comparisons. In Fig.6a it may be seen that predictions of these extinction strain rates depend strongly on the chemical-kinetic descriptions employed. The original San Diego mechanism over-predicts the extinction strain rates significantly, while the up-dated mechanism under-predicts them. For purposes of comparison, predictions of three other mechanisms[45,46,26] are shown in the figure. One of them[46] exhibits substantial over-predictions for fuel-lean conditions, the oldest[45] produces appreciable under-predictions, and the newest[26] gives even larger under-predictions. This last observation is especially noteworthy since that particular mechanism has been proven to exhibit the best agreement with experimental data for both flame speed and ignition delay time under gas-turbine conditions[6]; the fidelity of predictions thus depends strongly on the combustion conditions and on the combustion property tested. For the conditions of these experiments, the best overall agreement is provided by the new San Diego mechanism. The comparisons shown in Fig.6b, where a log scale is employed because of the strong dependence of the extinction strain rate on pressure, indicate that the relative performance of the old and new San Diego mechanisms remain about the same at elevated pressures.

3.4 | NO_x Formation

Concentration profiles have been measured by molecular-beam mass spectroscopy in low-pressure burner-stabilized flat flames from 50 mbar to 120 mbar, with ammonia mole fractions between 21 percent and 25 percent[47]. Oxygen-argon mixtures were employed instead of air to be sure that the measured nitrogen originated only from the ammonia, and hydrogen was added at mole fractions from 5 percent to 13 percent to approximate the NH_3/H_2 fuel mixtures of interest. To assess the fidelity of NO predictions of the new mechanism, computations of structures of burner-stabilized flames of these mixtures were performed for these pressures at an initial feed-stream temperature of 298 K. Comparisons of the predictions with the measurements are shown in Fig.7.

The experimental and computational results shown in Fig.7a indicate that the mole fraction of NO formed in the flame decreases as the pressure increases. Unlike NO, nitrous oxide concentrations (not shown) peak in the interior of the flame and decrease to essentially zero in the products, the computational profiles under-estimating these concentrations but agreeing with experiment within a factor of two. The predictions of the new mechanism appear in Fig.7a to agree with the measurements better than those of the original mechanism. Extending these comparisons for stiochiometric mixtures to lean and rich equivalence ratios at the lowest pressure, as shown in Fig.7b, yields a similar conclusion except for the fuel-lean mixture, where the original mechanism appears to perform better. Comparisons (not shown) also were made for stoichiometric mixtures at the lowest pressure with the hydrogen percentage ranging from 5% to 13%, giving results showing that NO concentrations increase

with increasing hydrogen content (corresponding, perhaps counter-intuitively†, to decreasing ammonia content) and producing agreements similar to those in Fig.7a, favoring the new mechanism. These comparisons, however, are not definitive in that, although the reactant mixtures are fed into the burner at 298 K, burner heating by the flame may produce a higher effective initial temperature, as would be suggested by reported thermocouple temperature profiles. Computations for higher initial temperatures produced, perhaps surprisingly‡, less NO production, accentuating disagreements. The alternative of employing measured temperature profiles in place of energy conservation, which could provide more definitive tests, unfortunately was not available.

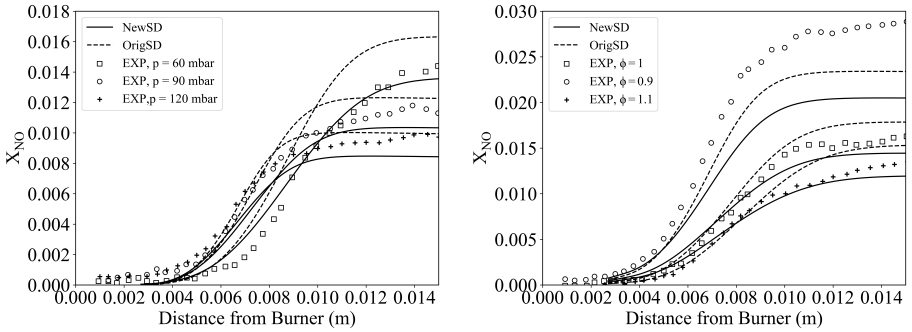

(a) $\phi = 1$, T = 298 K **(b)** p = 50 mbar, T = 298 K

FIGURE 7 Mole-fraction profiles of NO for mixtures with 25% NH_3 and 5% H_2, for three different pressures in stiochiometric mixtures and for three different equivalence ratios at 50 mbar and an inlet flow velocity of 0.42 m/s.

Finally, in the experiments[5] providing the points shown in Fig.3, measurements of NO in the exhaust also are reported, and results for the conditions of Fig.3b are plotted in Fig.8, along with computational predictions for freely propagating flames according to the new mechanism (which are practically the same as those of the original mechanism in this case). Although the agreement is close at an equivalence ratio of 1.1, the NO emission from the freely propagating flame decreases steeply with increasing equivalence ratios, as a consequence of the decreasing flame temperature reducing the NO production rate through the Zel'dovich mechanism (as well as the associated decrease in the pool of radicals needed to oxidize the nitrogen-containing fuel), while the measured emissions remain practically independent of the equivalence ratio. Since the propagating-flame predictions are readily explained, this notable difference may reflect additional chemistry occurring in the experiment subsequent to passage of the gas through the flame, somehow reducing NO under stoichiometric conditions (perhaps heterogeneously) and increasing it when the system is sufficiently fuel rich and the measured exhaust temperatures (always very subadiabatic) are higher.

4 | COMBUSTION BEHAVIOR OF AMMONIA-DERIVED FUELS AND COMPARISON WITH METHANE

In order to provide a first application of the updated kinetic scheme, we perform an evaluation of fundamental combustion properties for ammonia-based fuel blends relevant to gas-turbine applications and compare them with methane, a well-established gas-turbine reference fuel, focusing on initial temperatures of 750 K, which are typical of gas-turbine inlet temperatures. Early studies have illustrated, already several decades ago, some of the challenges emerging by substitution of ammonia to hydrocarbon fuels in gas turbines, due to the low reactivity and poor combustion characteristics of ammonia[3]. More recent investigations[48,49,50] have achieved some success in stabilizing ammonia-air flames in simplified laboratory models of gas-turbine combustors while, at the same time, reducing NOx and N_2O emissions to values closer to the regulatory limits. These advances have, however, been attained at the cost of a considerable increase of the fuel-air equivalence ratio (beyond stoichiometry) and

†Although the decreasing nitrogen content might be expected to decrease NO production, the increased branching through the hydrogen-oxygen chain, associated with there being more hydrogen in the fuel, increases the size of the radical pool that is responsible for NOx formation from the nitrogen-containing fuel, thereby causing more of the nitrogen to end up as NO and less as N_2, to an extent that overbalances the overall decrease in content of nitrogen.

‡The higher initial temperature increases the rate of fuel consumption, thereby decreasing the thickness of the reaction zone, so that fewer oxygen-containing radicals are present there, thereby lessening the NO production and allowing the N_2 production, which is less sensitive to temperature, to increase.

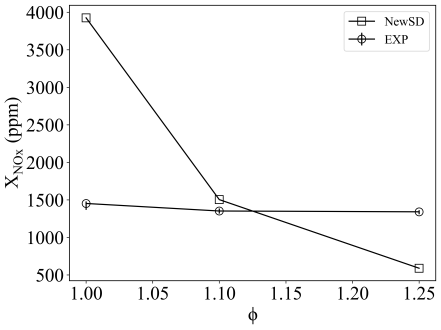

FIGURE 8 Variation of NOx emissions with the equivalence ratio for fuel-air mixtures of fuels having 50% NH_3/ 50% H_2 by volume.

of the residence time inside the combustion chamber, thereby raising possible issues with ammonia slip and reducing the fuel flexibility (fuel-switching capabilities) of the combustion system, respectively.

An interesting alternative to direct ammonia combustion is partial or complete ammonia dissociation ("cracking") to molecular hydrogen and nitrogen ($2\ NH_3 \rightarrow N_2 + 3\ H_2$) prior to combustion[3]. Complete ammonia dissociation provides a viable gas-turbine fuel, consisting of nitrogen-diluted hydrogen in a 3:1 ratio (by moles), with good potential in respect to flame stability and emissions. The mixture of 75% hydrogen and 25% nitrogen is characterized by increased heating value compared to neat ammonia (21.34 versus 18.6 MJ/kg), which is beneficial to the combustion process, but also by a relatively low Wobbe index compared with standard hydrocarbon fuels (about 10 MJ/Nm^3 versus 42-53 MJ/Nm^3), something that would negatively impact the fuel delivery system of the gas turbine and would require substantial changes. Irrespective of practical advantages and disadvantages of the resulting hydrogen/nitrogen mixture, a considerable amount of heat is required by the process of complete ammonia dissociation[51,52] or, alternatively, the oxidation of a non-negligible fraction ($\sim 7\%$) of the ammonia in the catalyst[53]. The required thermal energy can, in principle, be recovered from the gas turbine waste heat, but this withdraws it from the steam bottoming cycle (if present), lowering the overall efficiency of the power plant.

A more convenient solution that (partially) retains the combined-cycle efficiency is to design a combustion system that is able to optimally operate with a fuel mixture of hydrogen, nitrogen, and ammonia resulting from partial ammonia cracking. This approach can considerably reduce the sensible heat requirement of the dissociation process, depending on the share of ammonia that is retained. Furthermore, the resulting partial conversion of ammonia to hydrogen results in an enhancement of the overall reactivity of the fuel mixture[3] and, if such a mixture can be optimized in the right proportions of $NH_3/H_2/N_2$ to closely reproduce the combustion properties of natural gas, this opens the attractive possibility of retro-fitting existing gas turbines for operation with a carbon-free fuel with only minimal hardware modifications.

4.1 | Adiabatic Flame Temperature and Laminar Flame Speed

The present and following sections employ the updated chemical-kinetic scheme in numerical simulations focused on analysis of hydrogen/ammonia-air flames characterized by a fuel mixture that consists of 40% NH_3, 45% H_2 and 15% N_2 (by volume). This fuel blend, which corresponds to dissociation of 60% of the ammonia stream fed to the gas turbine (partial ammonia cracking) is chosen for the ammonia-derived fuel-blend composition because its combustion in air results in adiabatic flame temperatures T_{ad} and (unstrained) laminar flame velocities S_L that are close to typical values observed in methane-air combustion under gas-turbine conditions. Similarities in these key parameters, which play central roles in controlling gas-turbine performance and emissions of pollutants, are especially evident at fuel-lean conditions, as may be seen in Fig.9, which is based on calculations performed with Cantera, using the San Diego chemical-kinetic schemes for hydrocarbon and nitrogen chemistry (updated herein)at normal atmospheric pressure and a starting reactant temperature of 750 K. Although differences increase to some extent on the fuel-rich side, for combustion in air at an equivalence ratio $\phi = 0.45$, for example, both the ammonia-derived fuel blend and methane result in a flame temperature $T_{ad} \sim 1750K$. Also, the (unstrained) laminar flame velocity for the ammonia-derived fuel blend is reasonably close to that of the methane-air flame, exceeding it by approximately 30% (86 cm/s versus 66 cm/s).

Figure 10 further illustrates a number of similarities and differences between the structure of CH_4-air and $NH_3/H_2/N_2$-air flames. The net reaction-layer thickness for the main fuels is very similar for methane and for the ammonia-derived fuel blend

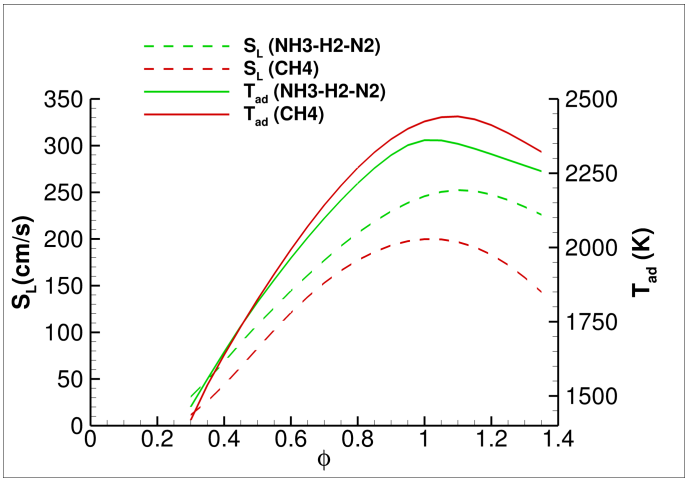

FIGURE 9 Calculated variation of the equilibrium adiabatic flame temperature and the laminar flame velocity with the equivalence ratio for methane-air mixtures and $NH_3/H_2/N_2$-air mixtures (the ammonia-derived fuel mixture is composed by 40% NH_3, 45% H_2 and 15% N_2 by volume.

at $\phi = 0.45$, as shown in Figs. 10a-10b, resulting in nearly identical flame thickness (0.579 versus 0.553 mm, respectively). Molecular hydrogen is, of course, only an intermediate species in the CH_4-air flame being formed and consumed within the flame reaction layer, while, on the other hand, it contributes considerably to the heat release in the $NH_3/H_2/N_2$-air flame. Furthermore, although hydrogen (net) consumption is initiated slightly upstream from that of ammonia, the hydrogen-consumption peak is, perhaps initially surprisingly, located downstream from the ammonia-consumption peak as a consequence of the additional hydrogen being released during ammonia consumption in steps 19 and 11.

In order to gain additional insight into the structure of $NH_3/H_2/N_2$-air flames, it is helpful to study these at near-stoichiometric and stoichiometric conditions for two different ammonia-derived fuel blends, 40% NH_3, 45% H_2 and 15% N_2 and 70% NH_3, 21% H_2 and 7% N_2. From the line plots in Figs. 10c-10f the following observations are made:

- The hydrogen reaction layer is (mostly) co-located with the ammonia reaction layer for all flames, with only a slight off-set in the downstream direction.
- As opposed to the lean case, at stoichiometric and near-stoichiometric conditions the hydrogen reaction rate is characterized by two peaks with an intermediate region of near-zero (net) consumption positioned between them, in correspondence of the ammonia consumption peak.
- The presence of the two-peaked structure in the hydrogen reaction layer is more evident in the flame with higher ammonia content in the fuel (Fig.10d).
- In spite of hydrogen's higher reactivity and faster kinetics, ammonia completely reacts in the flame reaction layer, and its mole fraction goes to zero in the products for all flames. On the other hand, hydrogen does not do so, and a non-zero mole fraction of hydrogen is present in the products for all flames at equivalence ratios between 1.1 and 0.9 (although, for the latter, in a very small concentration), consistent with its presence in the thermodynamic chemical-equilibrium composition at these adiabatic flame temperatures.

4.2 | Extinction Strain Rates in Laminar Counterflow Premixed Twin Flames

Direct Numerical Simulations (DNS) of twin laminar premixed flames in counterflow configurations on rectangular 2-D domains were performed with the S3D code[54] to complement the preceding comparative analysis. Although the effect of hydrogen addition in hydrocarbon flames and in CO-air flames has been studied extensively for premixed twin flames in counterflow configurations as reported in publications[55,56] from the group of Egolfopoulos and in references cited therein, the present study represents the first attempt to investigate this topic for combustion of ammonia/hydrogen/nitrogen-air blends in air.

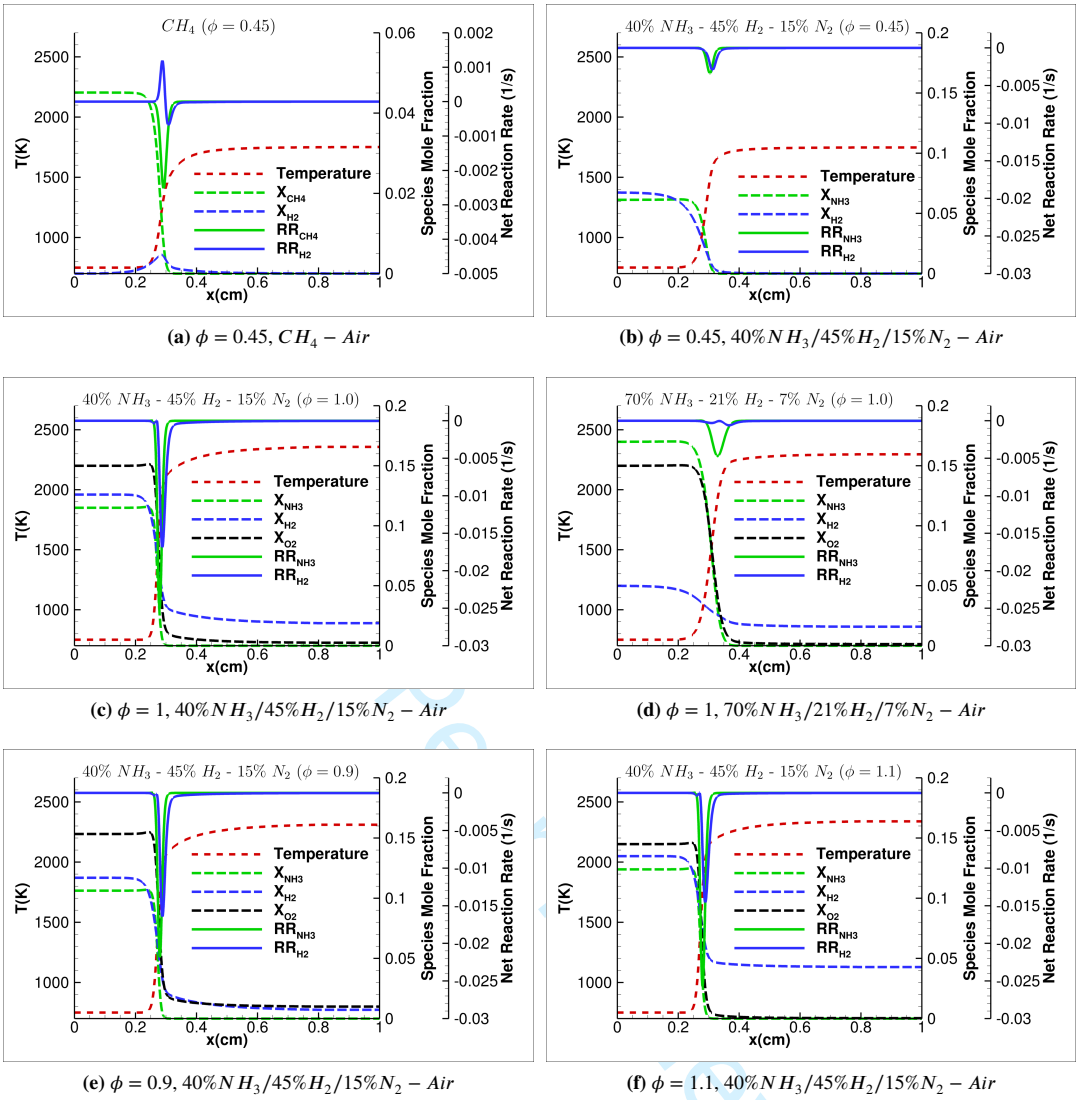

(a) $\phi = 0.45, CH_4 - Air$ **(b)** $\phi = 0.45, 40\%NH_3/45\%H_2/15\%N_2 - Air$

(c) $\phi = 1, 40\%NH_3/45\%H_2/15\%N_2 - Air$ **(d)** $\phi = 1, 70\%NH_3/21\%H_2/7\%N_2 - Air$

(e) $\phi = 0.9, 40\%NH_3/45\%H_2/15\%N_2 - Air$ **(f)** $\phi = 1.1, 40\%NH_3/45\%H_2/15\%N_2 - Air$

FIGURE 10 Flame structure for CH_4-air and $NH_3/H_2/N_2$-air flames at lean and near-stoichiometric conditions for an initial temperature of 750 K and a pressure of 1 atm.

4.2.1 | The Configuration

The two-dimensional physical domain represented in the computations spans a square of $L_x = 1$ cm by $L_y = 1$ cm in the Cartesian x- and y-directions, respectively. The Navier-Stokes equations for a reactive, multi-component, compressible fluid are discretized on a 400 x 400 Cartesian mesh, providing a spatial resolution of 25μm, which is sufficient to accurately resolve the flame structure and all diffusive, reactive, and dissipative scales of the reacting flow, even at the most severe level of strain applied. A mixture-averaged approximation is employed for the diffusion coefficients that are formulated in terms of the binary diffusion coefficients and the mixture composition, where the binary coefficient matrix is symmetric and the diagonal elements are zero. Furthermore, thermal diffusion (the Soret effect) is included in the formulation for the species diffusion velocities because of its relevant role in mixtures containing hydrogen. A fourth-order-accurate, six-stages-explicit, Runge-Kutta algorithm[57] is employed for time integration and the time step is fixed to 4 ns throughout the simulations. For additional details about the mathematical formulation adopted in the DNS code and the numerical methods employed therein see the reference paper on S3D published by the developer's group at Sandia[54]. All of the computations pertain to normal atmospheric inlet pressures.

Two initially flat premixed flames, in a back-to-back configuration, are positioned at the two longitudinal locations $x = 3$ mm and $x = 7$ mm, spanning the transverse y-direction, with combustion products located in between them. The flame structures,

for both the CH_4-air and the $NH_3/H_2/N_2$-air flames, are imported from 1-D ChemKin Premix solutions and applied to the 2-D DNS domain by a progress-variable mapping at the beginning of the simulations. The initial velocity field is set to zero (a quiescent fluid), and, upon start, a spatially uniform inward velocity in the x-direction at 750 K is imposed at the left and right domain boundaries, $x = 0$ mm and $x = 10$ mm, gradually increasing until the target values $U_{x0} = U_{st}$ and $U_{xL} = -U_{st}$ are reached, within approximately 1 or 2 ms that, therefore, represents the time duration of the initial transient. Outlet boundary conditions are imposed in the y-direction, at the bottom and top domain boundaries, $y = 0$ mm and $y = 10$ mm. Acoustically non-reflective inflow and outflow boundary conditions, according to the NSCBC methodology[54] adopted in S3D, are used for the domain inlet and outlet, respectively. The twin-flame counterflow configuration is qualitatively illustrated in Fig.11 which shows, as an example, the DNS solution from one of the configurations studied after stationarity is reached.

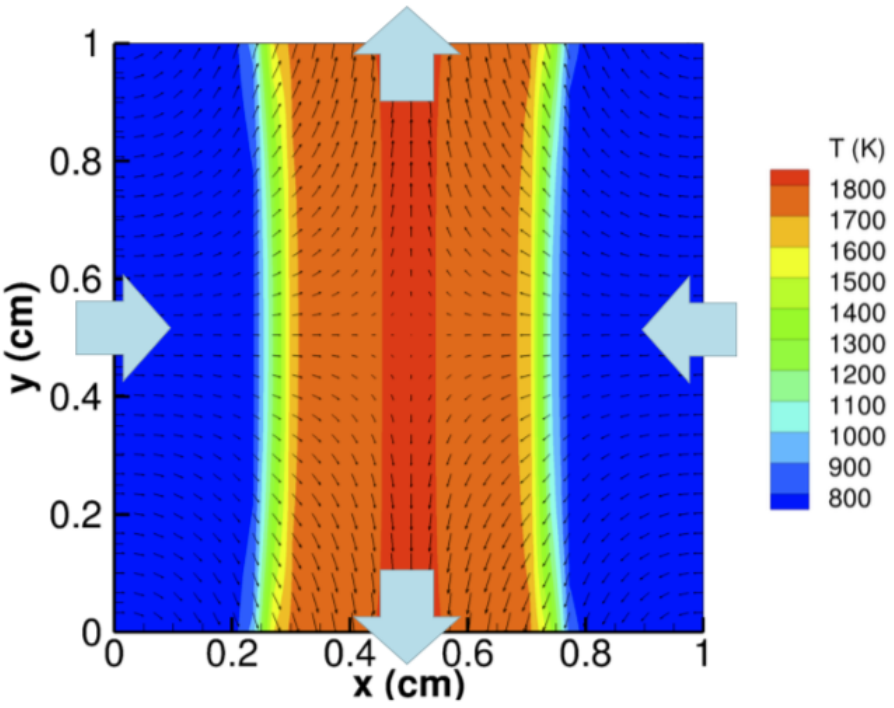

FIGURE 11 Illustration of the counterflow configuration and the positions of the twin flames.

4.2.2 | Comparison of Ammonia/Hydrogen/Nitrogen-Air Flames with Methane-Air Flames

The configuration described above ultimately results in a stagnation flow that acts on the premixed twin flames, straining them and reducing the thickness of the product layer between them. The distance between the peak heat-release rate of each flames will be denoted by D_{tf}. As higher values of U_{st} are imposed, the twin flames are increasingly strained and decreasingly able to sustain chemical reaction until, eventually, extinction takes place, at a value $U_{st} = U_{bo}$, where the latter subscript stands for blow-out. This is illustrated qualitatively in Fig.12, computed for an equivalence ratio of 0.45, which compares the final reactive flow fields of methane and ammonia/hydrogen/nitrogen flames after a stationary solution is reached for different values of the inlet velocity U_{st} at the inlet temperature of 750 K. Comparison of the top panels ($U_{st} = 3$ m/s) with the middle panels ($U_{st} = 8$ m/s) shows that the methane flame temperature decreases with increasing strain rate (defined as $a_{st} = 2U_{st}/L_x$) noticeably more rapidly than that of the blend. The two bottom panels show the temperature fields at the highest level of strain before the occurrence of extinction, corresponding to a significantly lower strain rate for methane, as implied by the different values of U_{st} that are listed in the figure. The value of U_{bo} is only 13 m/s for the methane flame, compared with 62 m/s for this ammonia-containing mixture, thereby exhibiting a difference of a factor of 5 in their extinction strain rates.

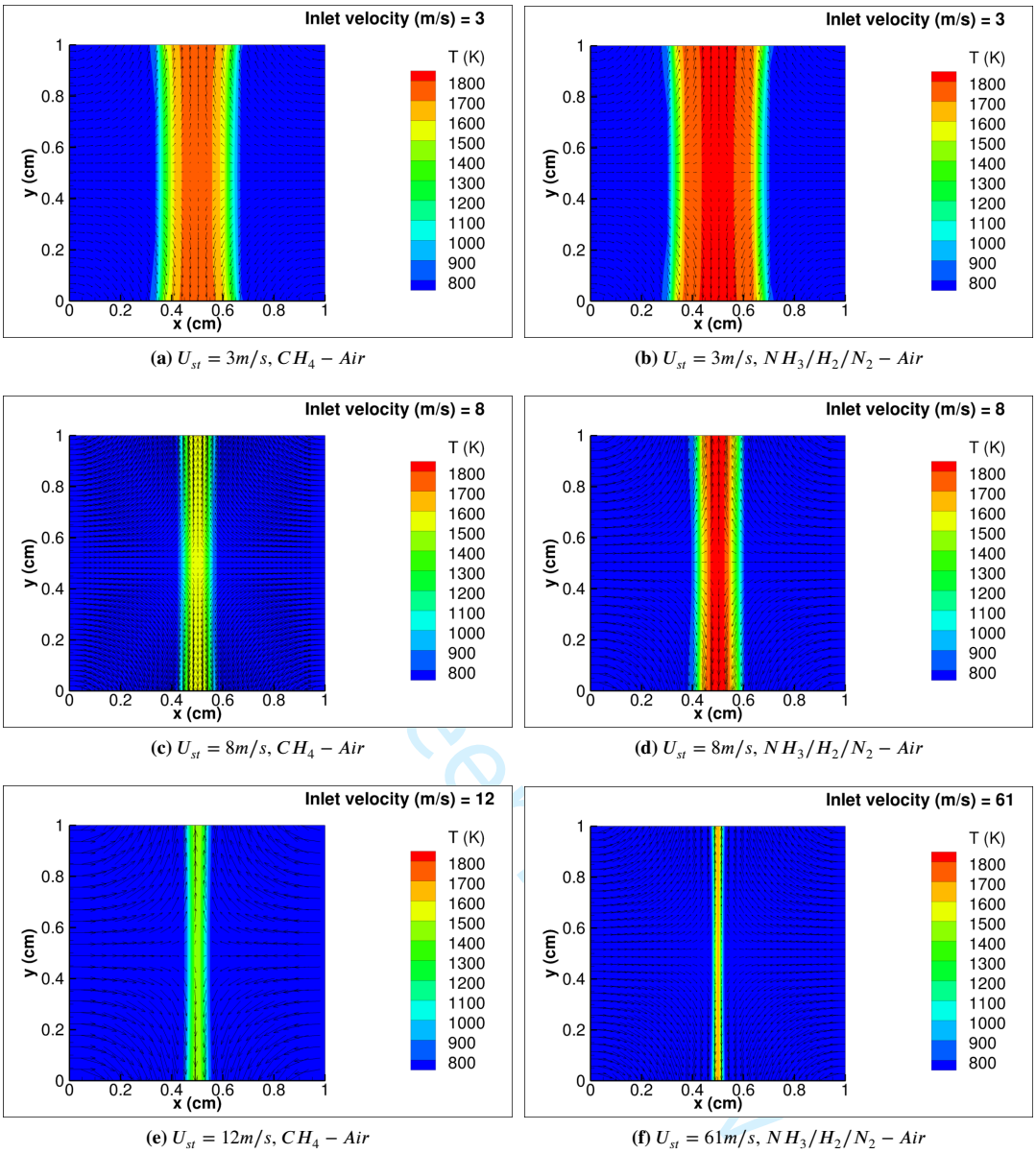

(a) $U_{st} = 3m/s, CH_4 - Air$ **(b)** $U_{st} = 3m/s, NH_3/H_2/N_2 - Air$

(c) $U_{st} = 8m/s, CH_4 - Air$ **(d)** $U_{st} = 8m/s, NH_3/H_2/N_2 - Air$

(e) $U_{st} = 12m/s, CH_4 - Air$ **(f)** $U_{st} = 61m/s, NH_3/H_2/N_2 - Air$

FIGURE 12 Stationary (final) DNS solutions of the counterflow twin-flame configurations for CH_4-Air (left) and $40\%NH_3/45\%H_2/15\%N_2$-Air (right) mixtures, with various inlet velocities U_{st}.

Figure 13 provides more quantitative information concerning the relationship between the rate of strain a_{st} imposed on the twin flames and the resulting distance between them D_{tf} (Fig.13a). In Fig.13b, the nondimensionlized version of these results, the inlet velocity U_{st} is normalized by the unstrained laminar flame speed S_L, and the data indicates that, while the methane flame blows out before the inlet velocities reach 20 times S_L, the ammonia/hydrogen/nitrogen flame is able to burn stably for U_{st} up to 70 times S_L. The distance between the flames is normalized by the unstrained laminar flame thickness δ_L in this figure, defined as the ratio of the difference between the burnt an unburnt temperatures to the maximum temperature gradient in the untrained laminar flame, and it is seen that methane-air combustion is able to support stable twin flames in the counterflow configuration only for values of this ratio greater than 3/4, but the ammonia/hydrogen/nitrogen-air twin flames are still burning stably for values of $D_{st} \sim 1/5$ of δ_L. This greater resistance to extinction cannot be attributed to the content of ammonia, which has been seen in Fig.6 to exhibit very low extinction strain rates, but instead is caused by the very high reactivity of the hydrogen component of the fuel blend, as well as the large value of the diffusion coefficient of hydrogen, which facilitates its

penetration into the high-temperature reaction region. The mixture that initially appears to be a good candidate for a drop-in fuel thus, largely because of its hydrogen content, is appreciably more blow-out resistant and so will be more robust in flame holding, which therefore require special consideration.

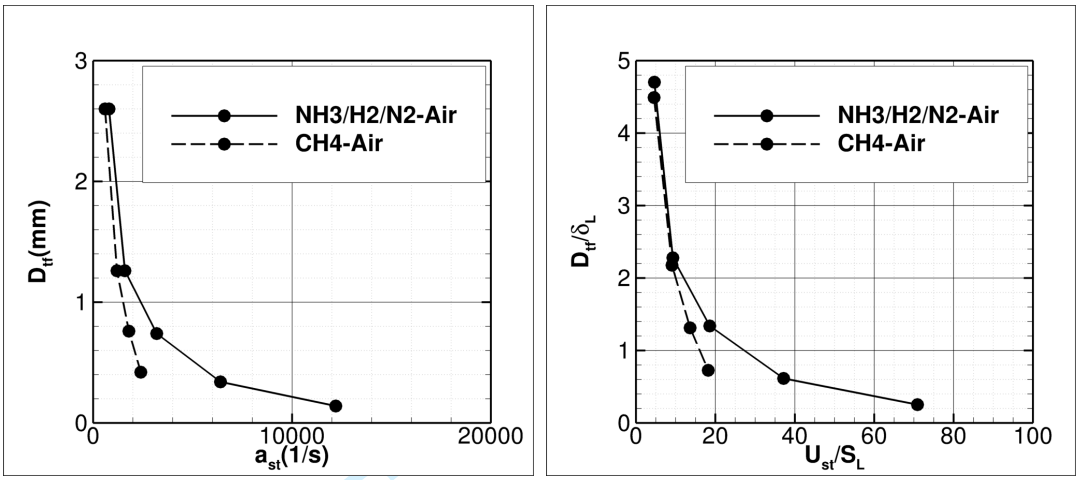

FIGURE 13 The distance between the twin flames D_{tf} versus strain rate a_{st} and inlet velocity U_{st}, both dimensional and nondimensional.

5 | CONCLUSIONS

The comparisons with experiment, summarized in the first six figures, serve to illustrate the degrees of accuracy that may be expected in employing this new short mechanism for nitrogen combustion chemistry. In an overall sense, the new mechanism provides a definite improvement over the original mechanism, especially with respect to predictions of ignition delay times. The accuracy achieved is likely to be sufficient for use in many investigations based on computational fluid dynamics. Application of this mechanism to considerations of ammonia-containing blends for use as drop-in fuels in gas turbines designed for natural gas shows that, when flame temperatures and burning velocities are matched by the blend, the carbon-free fuel is appreciably more resistant to extinction as a consequence of the high reactivity of its hydrogen content, which is an aspect that has to be taken into account in design considerations.

ACKNOWLEDGEMENT

The present research is supported by the CLIMIT-Demo program of the Research Council of Norway, Project Number 617137, BIGH2/Phase III - "Enabling safe, clean and efficient utilization of hydrogen and ammonia as the carbon-free fuels of the future" and by UNINETT Sigma2 Project Number nn9527k.

References

1. Abbas HF, Daud WW. Hydrogen production by methane decomposition: a review. *International journal of hydrogen energy* 2010; 35(3): 1160–1190.
2. Ursua A, Gandia LM, Sanchis P. Hydrogen production from water electrolysis: current status and future trends. *Proceedings of the IEEE* 2011; 100(2): 410–426.
3. Verkamp F, Hardin M, Williams J. Ammonia combustion properties and performance in gas-turbine burners. In: . 11. Elsevier. ; 1967: 985–992.
4. Valera-Medina A, Xiao H, Owen-Jones M, David W, Bowen P. Ammonia for power. *Progress in Energy and Combustion Science* 2018; 69: 63 - 102.
5. Li J, Huang H, Kobayashi N, He Z, Nagai Y. Study on using hydrogen and ammonia as fuels: Combustion characteristics and NOx formation. *International Journal of Energy Research* 2014; 38(9): 1214–1223.
6. Xiao H, Valera-Medina A. Chemical kinetic mechanism study on premixed combustion of ammonia/hydrogen fuels for gas turbine use. *Journal of Engineering for Gas Turbines and Power* 2017; 139(8): 081504.
7. Otomo J, Koshi M, Mitsumori T, Iwasaki H, Yamada K. Chemical kinetic modeling of ammonia oxidation with improved reaction mechanism for ammonia/air and ammonia/hydrogen/air combustion. *International Journal of Hydrogen Energy* 2018; 43(5): 3004–3014.
8. Petrova MV, Williams FA. A small detailed chemical-kinetic mechanism for hydrocarbon combustion. *Combustion and Flame* 2006; 144(3): 526–544.
9. Linteris GT, Williams F. Asymptotic and numerical analysis of a premixed laminar nitrogen dioxide-hydrogen flame. *Combustion Science and Technology* 1995; 105(4-6): 165–182.
10. Li S, Ilincic N, Williams F. Reduction of NOx formation by water sprays in strained two-stage flames. In: American Society of Mechanical Engineers. ; 1996: 836–843.
11. Li S, Williams FA. Formation of NOx, CH4, and C2 species in laminar methanol flames. In: . 27. Elsevier. ; 1998: 485–493.
12. Rørtveit GJ, Hustad JE, Li SC, Williams FA. Effects of diluents on NOx formation in hydrogen counterflow flames. *Combustion and Flame* 2002; 130(1-2): 48–61.
13. Rortveit G, Hustad J, Williams F. NOx Formations in Diluted CH4/H2 Counterflow Diffusion Flames. *International Journal of Energy for a Clean Environment* 2003; 4(4): 303–314.
14. Colorado A, McDonell V, Samuelsen S. Direct emissions of nitrous oxide from combustion of gaseous fuels. *International Journal of Hydrogen Energy* 2017; 42(1): 711–719.
15. Jiang Y, Gehmlich R, Knoblinger T, Seshadri K. Experimental and computational investigation of partially-premixed methoxymethane flames. *Combustion and Flame* 2018; 195: 99–104.
16. Miller JA, Bowman CT. Mechanism and modeling of nitrogen chemistry in combustion. *Progress in Energy and Combustion Science* 1989; 15(4): 287–338.
17. Klippenstein SJ, Harding LB, Glarborg P, Miller JA. The role of NNH in NO formation and control. *Combustion and Flame* 2011; 158(4): 774–789.
18. Glarborg P, Alzueta MU, Dam-Johansen K, Miller JA. Kinetic modeling of hydrocarbon/nitric oxide interactions in a flow reactor. *Combustion and Flame* 1998; 115(1-2): 1–27.
19. Miller JA, Glarborg P. Modeling the thermal De-NOx process: Closing in on a final solution. *International Journal of Chemical Kinetics* 1999; 31(11): 757–765.

20. Tsang W, Herron JT. Chemical kinetic data base for propellant combustion I. Reactions involving NO, NO2, HNO, HNO2, HCN and N2O. *Journal of Physical and Chemical Reference Data* 1991; 20(4): 609–663.

21. Baulch D, Bowman CT, Cobos C, et al. Evaluated kinetic data for combustion modeling: supplement II. *Journal of Physical and Chemical Reference Data* 2005; 34(3): 757–1397.

22. Meagher NE, Anderson WR. Kinetics of the O (3P)+ N2O reaction. 2. interpretation and recommended rate coefficients. *The Journal of Physical Chemistry A* 2000; 104(25): 6013–6031.

23. Mueller M, Yetter R, Dryer F. Kinetic modeling of the CO/H2O/O2/NO/SO2 system: Implications for high-pressure fall-off in the SO2+ O (+ M)= SO3 (+ M) reaction. *International Journal of Chemical Kinetics* 2000; 32(6): 317–339.

24. Dean AM, Bozzelli JW. Combustion chemistry of nitrogen. In: Springer. 2000 (pp. 125–341).

25. Davidson DF, Kohse-Höinghaus K, Chang AY, Hanson RK. A pyrolysis mechanism for ammonia. *International Journal of Chemical Kinetics* 1990; 22(5): 513–535.

26. Mathieu O, Petersen EL. Experimental and modeling study on the high-temperature oxidation of Ammonia and related NOx chemistry. *Combustion and Flame* 2015; 162(3): 554–570.

27. Dagaut P, Glarborg P, Alzueta MU. The oxidation of hydrogen cyanide and related chemistry. *Progress in Energy and Combustion Science* 2008; 34(1): 1–46.

28. Park J, Lin M. Laser-initiated NO reduction by NH3: Total rate constant and product branching ratio measurements for the NH2+ NO reaction. *The Journal of Physical Chemistry A* 1997; 101(1): 5–13.

29. Wolf M, Yang DL, Durant JL. Kinetic studies of NHx radical reactions. *Journal of Photochemistry and Photobiology A: Chemistry* 1994; 80(1-3): 85–93.

30. Goodwin D, Moffat HK, Speth RL. Cantera: An object-oriented software toolkit for chemical kinetics, thermodynamics, and transport processes. *Caltech, Pasadena, CA* 2009.

31. Pochet M, Dias V, Moreau B, Foucher F, Jeanmart H, Contino F. Experimental and numerical study, under LTC conditions, of ammonia ignition delay with and without hydrogen addition. *Proceedings of the Combustion Institute* 2019; 37(1): 621–629.

32. Song Y, Hashemi H, Christensen JM, Zou C, Marshall P, Glarborg P. Ammonia oxidation at high pressure and intermediate temperatures. *Fuel* 2016; 181: 358–365.

33. Zhang Y, Mathieu O, Petersen EL, Bourque G, Curran HJ. Assessing the predictions of a NOx kinetic mechanism on recent hydrogen and syngas experimental data. *Combustion and Flame* 2017; 182: 122–141.

34. Nakamura H, Hasegawa S, Tezuka T. Kinetic modeling of ammonia/air weak flames in a micro flow reactor with a controlled temperature profile. *Combustion and Flame* 2017; 185: 16–27.

35. Li J, Huang H, Kobayashi N, Wang C, Yuan H. Numerical study on laminar burning velocity and ignition delay time of ammonia flame with hydrogen addition. *Energy* 2017; 126: 796–809.

36. Lee J, Kim J, Park J, Kwon O. Studies on properties of laminar premixed hydrogen-added ammonia/air flames for hydrogen production. *International Journal of Hydrogen Energy* 2010; 35(3): 1054–1064.

37. Ichikawa A, Hayakawa A, Kitagawa Y, Somarathne KKA, Kudo T, Kobayashi H. Laminar burning velocity and Markstein length of ammonia/hydrogen/air premixed flames at elevated pressures. *International Journal of Hydrogen Energy* 2015; 40(30): 9570–9578.

38. Kumar P, Meyer TR. Experimental and modeling study of chemical-kinetics mechanisms for H2–NH3–air mixtures in laminar premixed jet flames. *Fuel* 2013; 108: 166–176.

39. Hayakawa A, Goto T, Mimoto R, Arakawa Y, Kudo T, Kobayashi H. Laminar burning velocity and Markstein length of ammonia/air premixed flames at various pressures. *Fuel* 2015; 159: 98–106.

40. Zakaznov V, Kursheva L, Fedina Z. Determination of normal flame velocity and critical diameter of flame extinction in ammonia-air mixture. *Combustion, Explosion, and Shock Waves* 1978; 14(6): 710–713.

41. Takizawa K, Takahashi A, Tokuhashi K, Kondo S, Sekiya A. Burning velocity measurements of nitrogen-containing compounds. *Journal of Hazardous Materials* 2008; 155(1-2): 144–152.

42. Pfahl U, Ross M, Shepherd J, Pasamehmetoglu K, Unal C. Flammability limits, ignition energy, and flame speeds in H2–CH4–NH3–N2O–O2–N2 mixtures. *Combustion and Flame* 2000; 123(1-2): 140–158.

43. Colson S, Hayakawa A, Kudo T, Kobayashi H. Extinction characteristics of ammonia/air counterflow premixed flames at various pressures. *Journal of Thermal Science and Technology* 2016; 11(3): 1–11.

44. Choi S, Lee S, Kwon OC. Extinction limits and structure of counterflow nonpremixed hydrogen-doped ammonia/air flames at elevated temperatures. *Energy* 2015; 85: 503–510.

45. Smith GP, Golden DM, Frenklach M, et al. GRI 3.0 Mechanism. *Gas Research Institute (http://www. me. berkeley. edu/gri_mech)* 1999.

46. Tian Z, Zhang L, Li Y, Yuan T, Qi F. An experimental and kinetic modeling study of a premixed nitromethane flame at low pressure. *Proceedings of the Combustion Institute* 2009; 32(1): 311–318.

47. Duynslaegher C, Jeanmart H, Vandooren J. Flame structure studies of premixed ammonia/hydrogen/oxygen/argon flames: experimental and numerical investigation. *Proceedings of the Combustion Institute* 2009; 32(1): 1277–1284.

48. Kurata O, Iki N, Matsunuma T, et al. Performances and emission characteristics of NH3-air and NH3-CH4-air combustion gas-turbine power generations. *Proceedings of the Combustion Institute* 2017; 36: 3351–3359.

49. Kurata O, Iki N, Inoue T, et al. Development of a wide range-operable, rich-lean low-NOx combustor for NH3 fuel gas-turbine power generation. *Proceedings of the Combustion Institute* 2019; 37: 4587–4595.

50. Okafor E, Somarathne K, Hayakawa A, et al. Towards the development of an efficient low-NOx ammonia combustor for a micro gas turbine. *Proceedings of the Combustion Institute* 2019; 37: 4597–4606.

51. Zhang Z, Liguori S, Fuerst TF, Way JD, Wolden CA. Efficient Ammonia Decomposition in a Catalytic Membrane Reactor To Enable Hydrogen Storage and Utilization. *ACS Sustainable Chemistry & Engineering* 2019; 7(6): 5975-5985.

52. Sato K, Abe N, Kawagoe T, Miyahara iS, Honda K, Nagaoka K. Supported Ni catalysts prepared from hydrotalcite-like compounds for the production of hydrogen by ammonia decomposition. *International Journal of Hydrogen Energy* 2017; 42(10): 6610 - 6617.

53. Nagaoka K, Eboshi T, Takeishi Y, et al. Carbon-free H(2) production from ammonia triggered at room temperature with an acidic RuO(2)/Îş-Al(2)O(3) catalyst. *Science advances* 2017; 3(4): e1602747–e1602747.

54. Chen JH, Choudhary A, Supinski dB, et al. Terascale direct numerical simulations of turbulent combustion using S3D. *Computational Science & Discovery* 2009; 2(1): 015001.

55. Vagelopoulos C, Egolfopoulos F. Laminar flame speeds and extinction strain rates of mixtures of carbon monoxide with hydrogen, methane, and air. *Symposium (International) on Combustion* 1994; 25(1): 1317 - 1323. Twenty-Fifth Symposium (International) on Combustion.

56. Long AE, Burbano H, Speth RL, Movaghar A, Egolfopoulos FN, Green WH. An apparatus-independent extinction strain rate in counterflow flames. *Proceedings of the Combustion Institute* 2019; 37(2): 1979 - 1987.

57. Kennedy CA, Carpenter MH, Lewis R. Low-storage, explicit Runge-Kutta schemes for the compressible Navier-Stokes equations. *Applied Numerical Mathematics* 2000; 35(3): 177 - 219.